

A Method for Establishing Tropospheric Atmospheric Refractivity Profile Model Based on Multiquadric RBF and k -means Clustering

Tao Ma, Heng Liu, and Yu Zhang

Abstract—A modeling method using multiquadric (MQ) radial basis function (RBF) and k -means clustering is proposed to establish the tropospheric atmospheric refractivity (TAR) profile model. The MQ-RBF interpolation algorithm is trained with the measurement data from 132 meteorological stations in 10 years. Mean Absolute Error (MAE) and Root Mean Squared Error (RMSE) of the prediction results are investigated with different local neighborhood parameters (r , θ , and t) of the MQ-RBF. Considering the tradeoff between RMSE and MAE, the parameters of the search ellipse (r , θ , and t) are optimized. The linear fit coefficients (a_1 , b_1 , a_2 , and b_2) of the linear relationships between the coefficients (C_1 and G) of TAR distribution formula and atmospheric refractive (N_0) at observation station are obtained by using the least square linear regression method with k -means clustering algorithm. This method overcomes the difficulty of measuring the TAR profile under various meteorological conditions at different time and place, and has the characteristics of real-time, convenient and accurate. It provides a promising method for the correction of TAR errors in the radar applications.

Index Terms—Tropospheric atmospheric refractivity, RBF, multiquadric, linear regression, k -means clustering

I. INTRODUCTION

Since radar was invented, it had played important roles in meteorological forecast, resource survey and supervision, Internet of things (IOT) industry, environmental monitoring and scientific researches on celestial bodies, atmospheric physics and ionospheric structure. The radar wave propagation path and phase angle of echo are greatly affected by the tropospheric atmospheric refractivity (TAR). Therefore, the refractivity correction methods are widely used to improve the accuracy of the radar detection. Traditional refractivity correction methods are classified into three groups: ray tracing method, radiometer method and simplified correction method. Compared with the first two

methods, simplified correction method has the advantages of short operation time and low cost. Hence, it is necessary to establish the atmospheric refractivity profile model within a short time. Simplified atmospheric refractivity profile models have been investigated extensively, for example, linear model, exponential model, double exponential model, Hopfield model and subsection model [1]-[3].

Recently, the refractivity in the tropospheric region is estimated using an artificial neural network (ANN) which use sigmoid transfer function as the activation function between the hidden and output layers [4]. The results show that the influence of the relative humidity on the refractivity is greater than that of other tropospheric parameters. A hybrid model based on the ANN with a genetic algorithm (GA) is proposed to solve the inversion problem of atmospheric refractivity estimation [5]. A propagation factor curve achieved by the hybrid method is closer to the reference one. As a special case of ANN, the RBF neural network has excellent features, such as universal approximation, compact topology, faster learning speed and excellent non-linear approximation capabilities [6]-[8]. Therefore, it is widely used for time series prediction, pattern recognition and complex mappings [9]-[14]. The RBF neural network method is also used to retrieve atmospheric extinction coefficients (AEC) in the lidar measurements [15]. The results confirm that the model established by the RBF neural network is better than the Fernald method in the aspect of speed and robustness. The MQ method has been proved to be an excellent interpolation method in terms of timing, storage, accuracy, visual pleasantness of the surface, and ease of implementation [16]-[18]. Moreover, the MQ-RBF is proposed as an effective numerical method for solving the science, engineering and economics problems, such as the heat conduction problems [19], radiative heat transfer problems [20], acoustic problems [21], elastic problems [22], options evaluation problems [23], and financial Heston-Hull-White (HHW) equation [24].

The k -means clustering algorithm is the simplest and widely used partitioning-based clustering technique due to its ease of implementation, simplicity, efficiency, and empirical success [25]. A new method based on Entropy-Maximizing theory is investigated to model the Origin-Destination (OD) distribution of taxi trips in Harbin city-China. In this method, the k -means clustering method is utilized to partition raw pick-up and drop-off location into different zones. The established taxi trips distribution model is beneficial to improve the efficiency of transportation planning and enhance the quality of taxi services [26]. To solve the

Manuscript received October 18, 2019; revised March 23, 2020. This work was supported in part by the scientific and technological project of Henan province under Grant 182102310712, the Key Project of Henan Education Department under Grant 19A510002 and the Ph. D. Program of Henan Normal University under Grant 5101239170010.

Tao Ma is with Henan Normal University and Key Laboratory Optoelectronic Sensing Integrated Application of Henan Province, Xinxiang, 453007 China (e-mail: matao79@bupt.edu.cn).

Heng Liu is with Henan Normal University and Academician Workstation of Electromagnetic Wave Engineering of Henan Province, Xinxiang, 453007 China. (corresponding author to provide phone: +8613462349935; e-mail: hengmaggie@163.com).

Yu Zhang is with Henan Normal University and Academician Workstation of Electromagnetic Wave Engineering of Henan Province, Xinxiang, 453007 China. (e-mail: hsdzhangyu@126.com).

problem of noise and nonlinearity in under water visible light communication systems, an algorithm based on k -means clustering is proposed to correct the phase deviation of special-shaped 8-QAM constellations [27]. A method based on the semi-supervised k -means and mean shift algorithm is used to detect the high-frequency oscillations (HFOs) in epileptic seizure onset zones (SOZs) localization. It is helpful for the accurate localization before clinical epilepsy surgery due to its good sensitivity and specificity [28]. In addition, the k -means algorithm is proposed to analyze commercial aircraft fuel consumption during descent [29], performance optimization of copy number variants (CNVs) [30], and classification of the different phases of an uninterrupted traffic flow [31]. An RBF neural network with k -Means clustering is also developed to establish the rainfall prediction model [32] and estimate the sound source angle [33].

In this paper, a method based on MQ-RBF and k -means clustering is proposed to fast establish the TAR profile model. The principle of the MQ-RBF and the flow chart of TAR profile modeling are introduced briefly. Then MAE and RMSE of the prediction results with different interpolation methods are studied and compared. The local neighborhood parameters of the MQ are optimized, and the TAR profiles in China are established and demonstrated.

The rest of the paper is organized as follows. Section II describes the Modeling Theory and Analysis Method of the MQ-RBF, including its principle and algorithm flow. In Section III, the performances of the MQ-RBF and parameters optimization are discussed, then TAR profiles are established. At last, conclusions are given.

II. MODELING THEORY AND ANALYSIS METHOD

The TARs at 132 meteorological stations in China are obtained by using the ten-year meteorological data which were measured by the method of balloon sounding. The geographic position distribution of the 132 stations in China is shown in Fig. 1.

In general, the atmospheric refractive index (n) is between 1.00026 to 1.00046 near the ground. It is usually represented as radio refractivity (or atmospheric refractivity, N) in radio band [34]. The flow chart of TAR profile modeling is shown in Fig. 2. The modeling of TAR profile is divided into 4 steps:

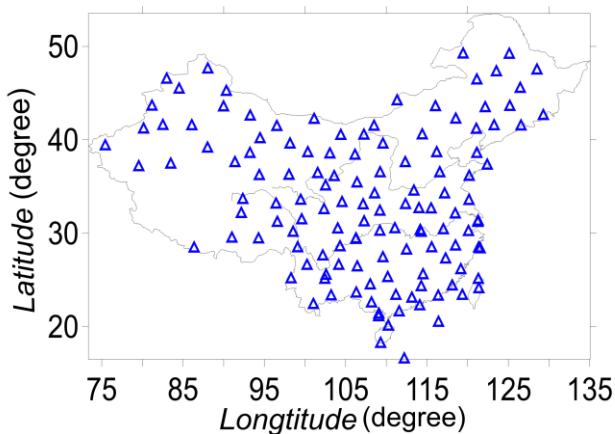


Fig. 1. Geographic position distribution of the 132 observation stations in China.

(1) Generation of the training dataset: the training dataset is established from the measurement data by using the piecewise model. Then the outlier data are removed from the training dataset according to the Pauta criterion. The training dataset can be updated to meet user needs.

(2) Prediction of the TAR coefficients: the gridding of the prediction region is firstly divided, and the initial parameters of the MQ method are set for predicting TAR coefficients of each grid node. Then, the MQ parameters are optimized by using the cross validation. The prediction dataset can be achieved and expressed as a matrix \mathbf{Z} .

(3) Linear regression optimization: the parameter k is determined according to the observation time in one day. The data in matrix are assigned to the closest initial cluster center. Then the centers are recalculated until the termination conditions are met. The linear regressions of the data after k -means clustering are achieved with least square method (LSM). The linear fit coefficients are obtained, which are used for the correction of TAR errors in the radar applications.

(4) Establishment of the TAR model profile: according to the ground refractive index and altitude measured by the instrument, the grid parameters and linear fit coefficients are determined. Then the TAR model is established, and it is compared with the measurement data to verify its accuracy and error.

The refractive index $N(h)$ with different altitude (h) is calculated by formula (1) at observation stations. The piecewise model is usually adopted to simulate the TAR at different altitudes, which is shown as

$$N(h) = \begin{cases} N_0 G(h - h_s) & h_s \leq h \leq h_s + H_1 \\ N_1 \exp[-C_1(h - h_s - 1)] & h_s + H_1 < h \leq H_9 \\ N_9 \exp[-C_9(h - 9)] & h > H_9 \end{cases}, \quad (1)$$

where h_s is the altitude of the observation station, $H_1=1$ km, $H_9=9$ km. N_0 , N_1 , and N_9 are the atmospheric refractive indices at h_s , H_1 , and H_9 , respectively. G is the vertical gradient of the atmospheric refractive index within 1 km above the ground. C_1 is the exponential attenuation coefficient of the atmospheric refractive index when h is between h_s+H_1 and H_9 . C_9 is the exponential attenuation coefficient of the atmospheric refractive index when h is higher than H_9 . The annual mean of $C_9=0.1434$ is widely used because the atmospheric state parameters above the altitude of 9 km are nearly unchanged. The ten-year N_0 , G , and C_1 of the atmospheric refractive index model at 132 observation stations are obtained by using the piecewise model, which are chosen as the training dataset. The training dataset is expressed as an $m \times 3$ matrix \mathbf{A}_{tr} , where m is the number of the coefficient set (N_0 , G , and C_1). The outlier data are removed from the \mathbf{A}_{tr} based on the Pauta criterion.

In order to establish the TAR profile model, rectangular grids are used. China covers a vast territory and its atmospheric environment range from 70°E to 135°E, and 15°N to 55°N. The N_0 , G , and C_1 at 5,346 grid nodes are predicted by using the MQ-RBF interpolation method at a 1° longitude interval and 0.5° latitude interval.

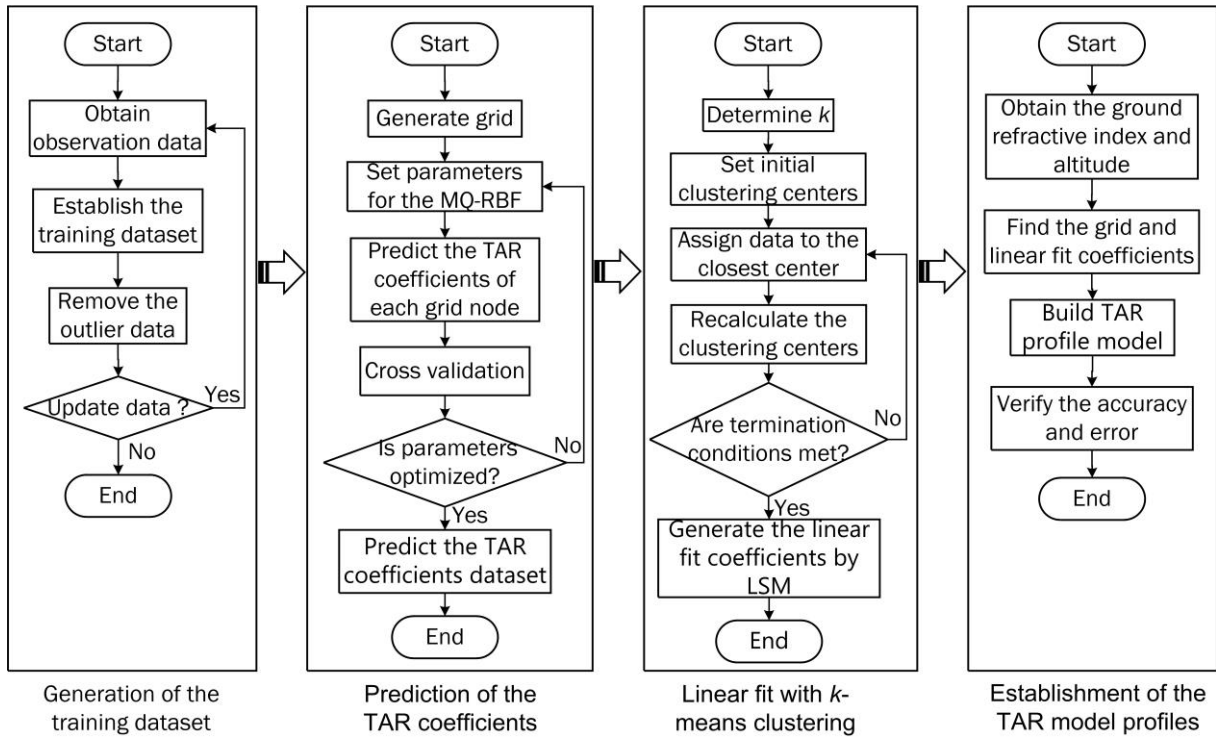


Fig. 2. Flowchart of the TAR profile modeling with the multiquadric RBF and k -means clustering.

The MQ-RBF method is looking for an appropriate function $s(x)$ to describe the relationship between x and f_k in a given dataset $\{x, f_k\}$, ($k=1, 2, \dots, n$), namely, $s(x)=f_k$, where $s(x)=\sum_{k=1}^N c_k \Phi(\|x-x_k\|)$. The multiquadric function is used as the basis kernel function of the RBF due to the high accuracy and smoothness in the interpolation applications. The multiquadric function shows as formula (2).

$$\Phi(r) = (r^2 + \gamma^2)^\beta, \quad (2)$$

where γ and r are the shaping factor and the space radius of the RBF, respectively. The value of γ^2 controls the smoothness of $s(x)$, which is calculated by the numerical method which decides the weight of the edge point. A small γ makes $\Phi(r)$ change sharply along the radial direction from the center point (the grid node to be predicted) and leads to overfit. And r is the relative distance from the center point to the training sample nodes, which has a great impact on the predicted value of the grid node. Here, β is 0.5, γ^2 is calculated by the formula of $L^2/(25 \times N)$, L is the length of diagonal of the data extent, N is the number of training samples.

The predicted value \mathbf{Z} could be N_0 , G , or C_1 , which is obtained by

$$\mathbf{Z}(x, y) = \sum_{k=1}^N \omega_k \Phi_k(x, y), \quad (3)$$

where x and y are respectively the longitude and latitude values of the geographical coordinates. Here, r in formula (2) is replaced by $\|(x, y) - (x_k, y_k)\|$. The predicted values at grid nodes are put in a M by 1 matrix $\mathbf{Z} = (Z_1, Z_2, \dots, Z_M)^T$, M is the number of the grid nodes to be predicted. \mathbf{Z} can be expressed as $\mathbf{Z} = \Phi \cdot \omega$, where Φ is a M by M matrix of the multiquadric functions. $\omega = (\omega_1, \omega_2, \dots, \omega_M)^T$ is a M by 1 matrix of the weight coefficients.

To verify the accuracy of the proposed algorithms, the leave-one-out cross validation is adopted. The sample set is

divided into two groups: one is training set, the other is validation set. After training with the training set, the predicted data are obtained and compared with the measurement data in the validation set. Then MAE and RMSE are calculated to evaluate the accuracy of the prediction results, which are expressed as

$$\text{MAE} = \frac{1}{N} \sum_{i=1}^N |Z_i - Z_{i0}| \quad (4)$$

$$\text{RMSE} = \sqrt{\frac{1}{N} \sum_{i=1}^N (Z_i - Z_{i0})^2} \quad (5)$$

where Z_{i0} and Z_i are the measured and predicted values of the i -th station, respectively. N is the number of the observation stations for verification. The MAE reflects the overall error or precision level of the prediction results, and RMSE reflects the sensitivity and extreme value of the estimated value of the sample data.

III. TAR PROFILE MODELING AND ANALYSIS

A. Coefficients Model of the TAR profile

The modeling of the coefficients of TAR profile is based on the sample data at 12:00 on 26 January 1995. The distribution of the predicted coefficients (N_0 , C_1 , and G) are simulated as shown in Figs. 3(a)-3(c).

In Fig. 3(a), N_0 is between 170 and 380. N_0 of the eastern coastal area is higher than that of west area in China, because the eastern coastal area belongs to the monsoon climate affected by the Marine climate greatly. The air humidity is high due to abundant rainfall, which leads to the increase of N_0 . The western China mostly belongs to continental climate, which is mostly arid or semi-arid region. Due to the lack of precipitation and the low content of water vapor in the air, N_0 is much smaller than that in the eastern regions. Especially in the region between 85°E to 95°E and 25°N to 35°N , it belongs to the plateau mountain climate, the average altitude

is higher than 2000 meters. The low air temperature and low air pressure lead to the sharp decrease of the N_0 .

The contour distribution C_1 of and G are shown in Figs. 3(b) and 3(c), respectively. C_1 and G change greatly in the southeast of China, while change slowly in the northwest of China. The reason is the same as above.

B. Error comparison

For comparison, MAE and RMSE of the prediction results by using the Multiquadric (MQ) method are investigated with other 7 different methods which are Kriging (KG), Modified Shepard's Method (MSM), Triangulation with Linear Interpolation (TLI), Natural Neighbor (NAN), Minimum Curvature (MC), Nearest Neighbor (NEN), and Inverse Distance to a Power (IDP). RMSE and MAE with different methods are shown in Figs. 4(a)-4(c).

For N_0 , RMSE and MAE of the MQ are 8.3652 and 5.7945, respectively. The MQ has the smallest RMSE and MAE among the 8 methods. The discreteness of the predicted N_0 deviates from the measured value is smallest, and the overall error level is the best one. For C_1 , RMSE and MAE of the MQ are close to that of the KG and NAN, but smaller than other methods. For G , RMSE of MQ and TLI are similar and

superior to other methods, while the MAE is comparable to other methods. RMSE and MAE of the prediction results simulated by 8 methods are shown in TABLE 1.

C. Parameter optimization of the MQ-RBF

The MQ interpolation algorithm is better than the other 7 algorithms. Using the MQ as the radial basis kernel function, the capability of prediction results mainly depends on its basic parameters of the local neighborhood (e.g., search circle or search ellipse). The atmospheric refractive index distribution is a natural phenomenon which is caused by the physical processes. It has a preferred orientation, such as the direction parallel to the coastline in China. Hence, the search ellipse is used as the local neighborhood for prediction of the grid nodes. Data in the search ellipse determine the value of a grid node at the center of the search ellipse, however the data outside are ignored. Excessive neighborhood selection will contain some data without correlation degree, while smaller neighborhood will lead to no correlation data in the neighborhood. Therefore, the neighborhood parameters greatly affect the accuracy of the prediction results. Usually, data closer to the grid nodes have more weight than those farther from the grid nodes.

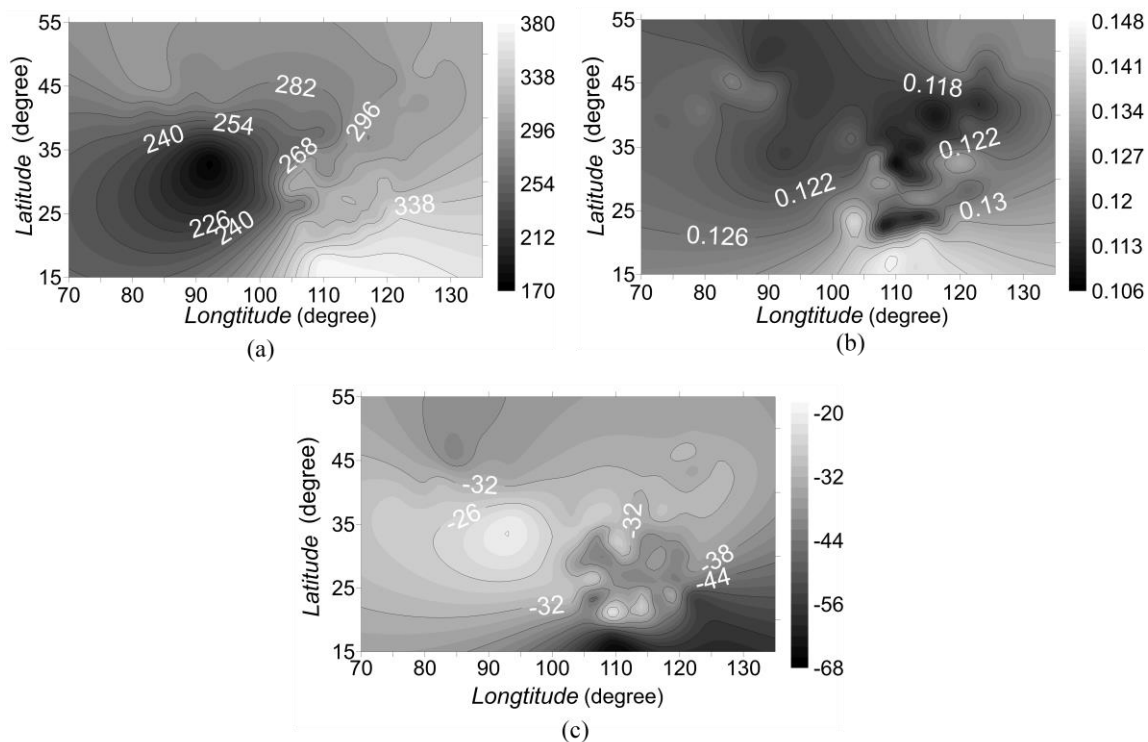


Fig. 3. Contour distributions of (a) N_0 , (b) C_1 , and (c) G .

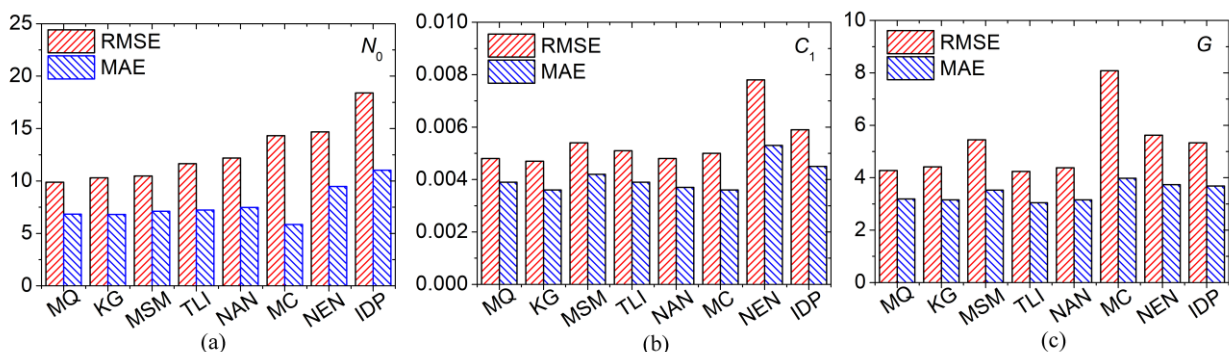


Fig. 4. Comparison of RMSE and MAE for N_0 , C_1 , and G with 8 interpolation methods.

TABLE 1
RMSE AND MAE OF N_0 , C_1 AND G WITH 8 INTERPOLATION METHODS

Interpolation Function	RMSE			MAE		
	N_0	C_1	G	N_0	C_1	G
Multiquadric (MQ)	8.3652	0.0048	4.2588	5.7945	0.0038	3.1648
Kriging (KG)	10.3001	0.0047	4.4156	6.8071	0.0036	3.1540
Modified Shepard's Method (MSM)	10.4758	0.0054	5.4477	7.1084	0.0042	3.5290
Triangulation with Linear Interpolation (TLI)	11.6469	0.0051	4.2397	7.2327	0.0039	3.0435
Natural Neighbor (NAN)	12.1926	0.0048	4.3790	7.4810	0.0037	3.1568
Minimum Curvature (MC)	14.3241	0.0050	8.0811	5.8547	0.0036	3.9809
Nearest Neighbor (NEN)	14.6841	0.0078	5.6189	9.4707	0.0053	3.7378
Inverse Distance to a Power (IDP)	18.4021	0.0059	5.3297	11.0335	0.0045	3.6802

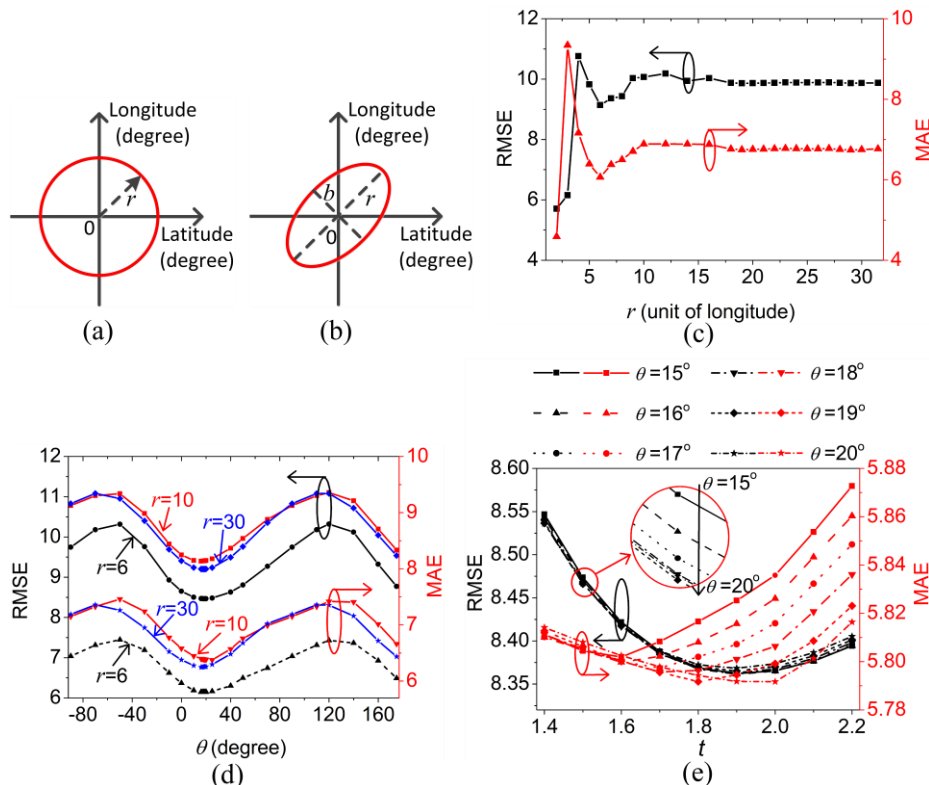


Fig. 5. (a) search circle and its parameters, (b) search ellipse and its parameters, RMSE and MAE with different (c) r , (d) θ , and (e) t .

In order to optimize the performance of the MQ-RBF, RMSE and MAE with different local neighborhood parameters are studied. The main parameters of the search ellipse and search circle are shown in Figs. 5(a) and 5(b), respectively. The major axis of the search ellipse is set as same as the radius of the search circle (r), its unit is as same as longitude. The ratio of major and minor axes is r/b . θ is the angle between the major axis and the horizontal axis. Taking the prediction of N_0 as an example, the influences of r , θ and t on RMSE and MAE are discussed. For the search circle as shown in Fig. 5(c), the smallest RMSE and MAE are achieved when r is less than 4. However, small r leads to no correlation data for the grid nodes to be predicted, which make RMSE and MAE incorrect. The second smallest RMSE and MAE are obtained when r is ~ 6 . RMSE and MAE change slowly when r is greater than 10, because the prediction values of the grid nodes with the MQ-RBF method mainly

depend on the data near the nodes.

For the search ellipse, the influences of θ and t on RMSE and MAE are investigated. In Fig. 5(d), RMSE and MAE periodically change with θ when t is 1.5 due to the periodically change of θ . There are minimum RMSE and MAE when θ is 19° . The selection of θ is in accordance with the climate distribution in China. Both RMSE and MAE have a minimum when r is 6. When r of 6, the variations of RMSE and MAE with t are simulated and shown in Fig. 5(e). RMSE has a minimum when $t=1.9$, and changes slowly when θ varies from 15° to 19° . However, the MAE shows little change when t is less than 1.6, while it changes greatly when t is greater than 1.6. The value of t corresponding to the smallest MAE varies from 1.6 to 2.0. Considering the tradeoff between RMSE and MAE, $r=6$, $\theta=19^\circ$ and $t=1.9$ are chosen as the optimized parameters of the MQ-RBF method.

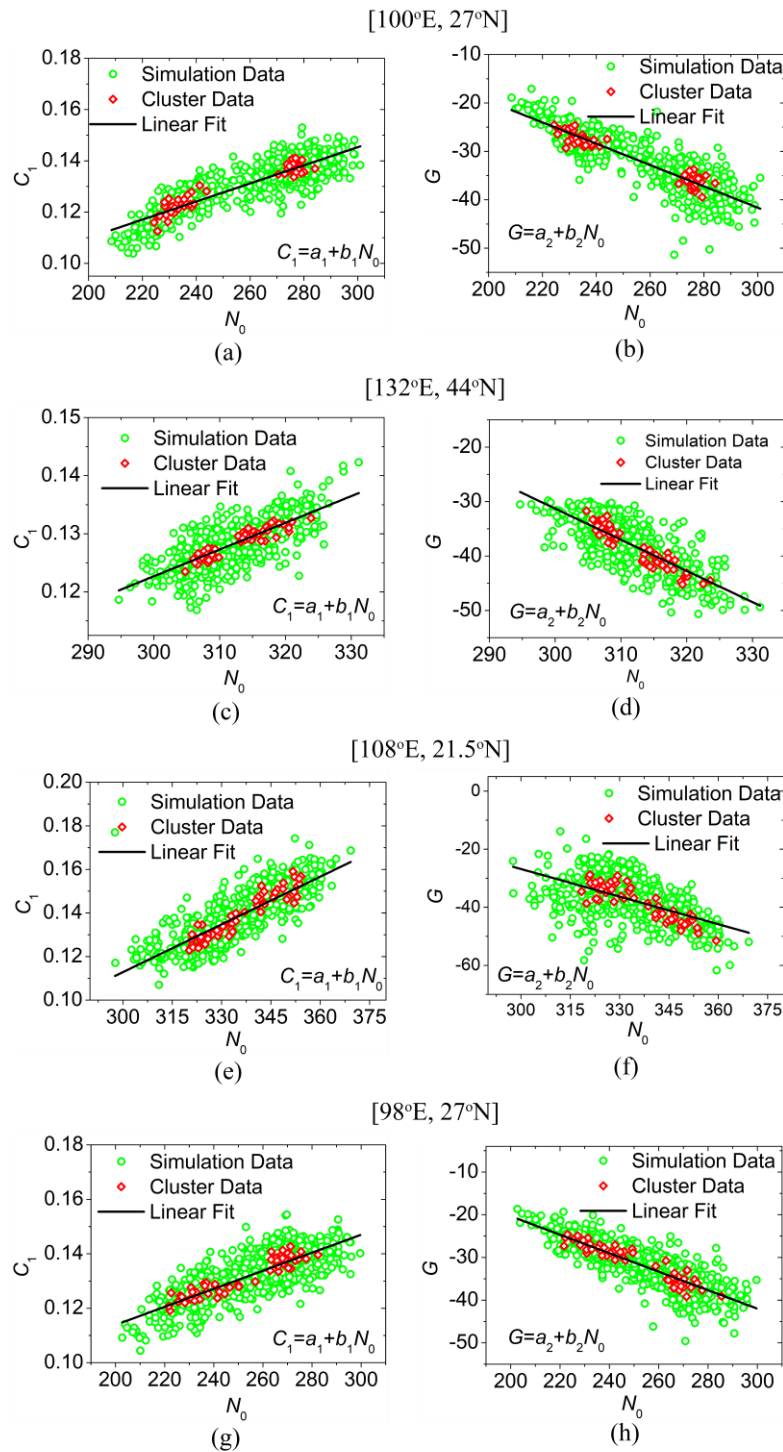


Fig. 6. Linear fit optimized by k -means clustering method, the linear fit of (a) C_1 and (b) G at the grid node [100°E, 27°N], the linear fit of (c) C_1 and (d) G at the grid node [132°E, 44°N], the linear fit of (e) C_1 and (f) G at the grid node [108°E, 21.5°N], the linear fit of (g) C_1 and (h) G at the grid node [98°E, 27°N].

TABLE 2
LINEAR FIT COEFFICIENTS AND DETERMINATION COEFFICIENTS OF C_1 AND G

Longitude	Latitude	C_1			G		
		a_1	b_1	R^2	a_2	b_2	R^2
100°E	27°N	0.040527	0.000350	0.920773	21.168072	-0.207652	0.933147
132°E	44°N	-0.010669	0.000445	0.877651	184.07320	-0.712291	0.902551
108°E	21.5°N	-0.154016	0.000871	0.902876	124.73015	-0.485488	0.830441
98°E	27°N	0.044068	0.000345	0.874978	25.439297	-0.226326	0.897084

D. linear regression optimized by k-means

In engineering applications, real-time radio wave refraction error correction is mainly used to improve radio instrumentation accuracy. Therefore, it is necessary to establish relationships between the parameters (C_1 and G) of the TAR profile model and N_0 . In order to obtain the TAR quickly and accurately, a linear regression method optimized by k -means clustering algorithm is proposed for C_1 and G fitting. Then we take the January data for 10 years in 5,346 grid nodes as an example. The parameter k is chosen as 2 since there are only two observation moments in each day. For each grid node, the groups (N_0, G) and (N_0, C_1) in a month are set as the data groups before clustering. New data groups could generate according to the k -means clustering algorithm. Then the least square method is used to achieve the linear fit for the data groups after clustering. The linear relationships between C_1, G and N_0 are respectively expressed as $C_1 = a_1 + b_1 N_0$ and $G = a_2 + b_2 N_0$, where a_1, b_1, a_2 and b_2 are the linear fit coefficients. The prediction data at the grid nodes [100°E, 27°N], [132°E, 44°N] and [108°E, 21.5°N], [98°E, 27°N] are choose for clustering and linear fit as shown in Fig. 6. Their linear fit coefficients a_1, b_1, a_2, b_2 and determination coefficients R^2 are listed in TABLE 2.

To verify the accuracy of the TAR model, the comparison of prediction results and relevant measurement data of 6 test stations are studied. The 6 test stations are Shenyang (SY),

Harbin (HEB), Hailar (HLE), Ejn Qi (EJNQ), Taroom (TAM), and TogtonHe (TTH). Their parameters (longitude, latitude, grid node, observation time, N_0 and h_s are listed in TABLE 3.

E. TAR profile model

The TAR model could be obtained by using the linear fit coefficients. The prediction data and measurement data with different altitude of the 6 observation stations are shown in Figs. 7(a)-7(f). The black solid lines are the prediction data built with the linear fit coefficients which obtained by the method based on MQ-RBF and k -means clustering. The red stars represent the observation data at the observation stations. In order to evaluate the error between the prediction data and observation data, MAE and RMSE are calculated as shown in Fig. 8. Smaller MAE and RMSE are achieved at TAM and TTH stations which have higher altitudes. Because the high altitude reduces the influence of the tropospheric region, which makes the prediction data more accurate. When $h_s \geq 9$ km, MAE and RMSE are smaller than those when $h_s < 9$ km. It proves that the TAR model agrees well with the observation data when the altitude is over 9 km. The reason is that the atmosphere over 9 km is the stratosphere which is cloudless and rarely changes in weather. On the contrary, at the altitude of below 9 km, the agreement between the TAR model and the observation data is not as good as that at the altitude of over 9 km.

TABLE 3
TEST STATION WITH GEOGRAPHICAL LOCATION, GROUND REFRACTIVE INDEX AND ALTITUDE

Test Station	Longitude	Latitude	Grid Node	Observation time	N_0	h_s
Shenyang (SY)	123.24	41.47	[123, 42.5]	1995012800	316.6	42
Harbin (HEB)	126.46	45.45	[126, 45.5]	1995 01 27 12	312.2	147
Hailar (HLE)	119.45	49.13	[119, 49]	1995011400	299.4	613
Ejin Qi (EJNQ)	101.13	42.15	[101, 42]	1995 01 27 12	269.8	936
Taroom (TAM)	94.38	36.12	[94, 40]	1994 01 31 12	217.7	2806
TogtonHe (TTH)	92.37	33.57	[92, 33.5]	1992011612	176.5	4555

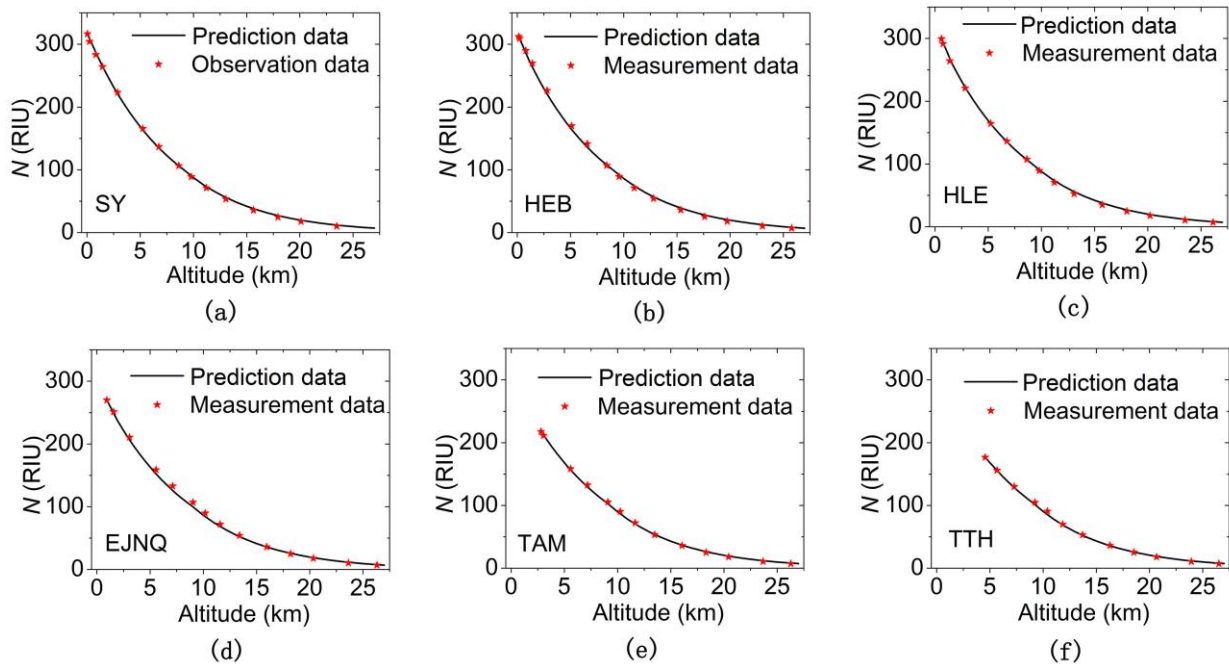


Fig. 7. Comparisons of the TAR prediction data and measurement data at the test stations.

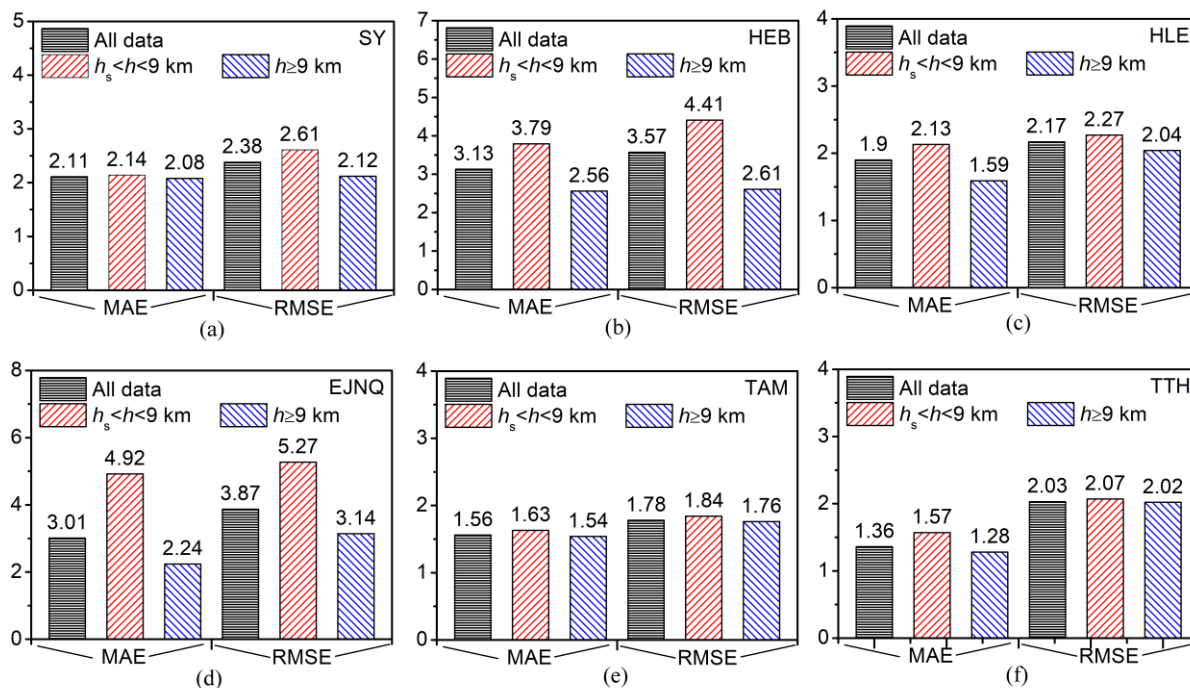


Fig. 8. MAE and RMSE between the TAR prediction data and measurement data at the test stations.

IV. CONCLUSIONS

In this paper, a method for establishing the TAR profile model based on the MQ-RBF algorithm is proposed, and the coefficients for wave refraction error correction are obtained with the least square linear regression method optimized by *k*-means clustering algorithm. The parameters N_0 , C_1 , and G for the 5,346 grid nodes are predicted by using the 10-year observation data at 132 stations in China. The cross-validation results show that RMSE and MAE are optimized when $r=6$, $\theta=19^\circ$, and $t=1.9$. The linear fit coefficients a_1 , b_1 , a_2 and b_2 between C_1 , G and N_0 are achieved to establish the TAR profile models. The measurement data of 6 observation stations are used to compare with the prediction data. It shows that the prediction and measurement data are consistent with each other. The relation coefficients a_1 , b_1 , a_2 and b_2 can be used to correct the refractive error of radio waves fast and in real-time. The atmospheric refractive index at different altitudes at any site can be predicted using the corresponding coefficients a_1 , b_1 , a_2 and b_2 , and N_0 . The proposed method has promising applications in the fields of satellite measurement and control system, navigation and positioning system, geodetic precision measurement, and astronomical measurement.

References

[1] S. J. Salamon, H. J. Ansen, H. D. Abbott, "Modelling radio refractive index in the atmospheric surface layer," *Electronics Letters*, vol. 51, no. 14, pp. 1119-1121, Jul. 2015.

[2] B. R. Bean, G. D. Thayer, "Models of the atmospheric radio refractive index," *Proceedings of the IRE*, vol. 47, no. 5, pp. 740-755, May 1959.

[3] H. S. Hopfield HS, "Two-quartic tropospheric refractivity profile for correcting satellite data," *Journal of Geophysical Research*, vol. 74, no. 18, pp. 4487-4499, Aug. 1969.

[4] G. F. Ibeh, G. A. Agbo, "Estimation of tropospheric refractivity with artificial neural network at Minna, Nigeria," *Global Journal of Science Frontier Research*, vol. 12, no. 1, pp. 9-14, May 2012.

[5] C. Tepecik, I. Navruz, "A novel hybrid model for inversion problem of atmospheric refractivity estimation," *AEU - International Journal of Electronics and Communications*, vol. 84, pp. 258-264, Feb. 2018.

[6] J. Park, I. Sandberg, "Universal approximation using radial-basis-function networks," *Neural Computation*, vol. 3, no. 2, pp. 246-257, Mar. 1991.

[7] T. Poggio, F. Girosi, "Networks for approximation and learning," *Proceedings of the IEEE*, vol. 78, no. 9, pp. 1481-1497, Sep. 1990.

[8] C. M. Lee, C. N. Ko, "Time series prediction using RBF neural networks with a nonlinear time-varying evolution PSO algorithm," *Neurocomputing*, vol. 73, no. 1-3, pp. 449-460, Dec. 2009.

[9] A. D. Dubey, "K-Means based radial basis function neural networks for rainfall prediction," in *2015 International Conference on Trends in Automation, Communications and Computing Technology*, Bangalore, 2015, p. 16091616.

[10] D. W. Chen, "Research on traffic flow prediction in the big data environment based on the improved RBF neural network," *IEEE Transactions on Industrial Informatics*, vol. 13, no. 4, pp. 2000-2008, Aug. 2017.

[11] D. F. Wei, "Network traffic prediction based on RBF neural network optimized by improved gravitation search algorithm," *Neural Computing and Applications*, vol. 28, no. 8, pp. 2303-2312, Aug. 2017.

[12] B. H. Chen, S. C. Huang, C. Y. Li, S. Y. Kuo, "Haze removal using radial basis function networks for visibility restoration applications," *IEEE Trans Neural Netw Learn Syst.* vol. 29, no. 8, pp. 3828-3838, Aug. 2017.

[13] S. K. Satapathy, S. Dehuri, A. K. Jagadev, "EEG signal classification using PSO trained RBF neural network for epilepsy identification," *Informatics in Medicine Unlocked.*, vol. 6, pp. 1-11, 2017.

[14] Kanojia MG, Abraham S. Breast cancer detection using RBF neural network. *International Conference on Contemporary Computing and Informatics, IEEE.* 2017; Greater Noida.

[15] H. X. Li, J. H. Chang, F. Xu, B. G. Liu, Z. X. Liu, L. Y. Zhu, Z. B. Yang, "An RBF neural network approach for retrieving atmospheric extinction coefficients based on lidar measurements," *Applied Physics B*, vol. 124, no. 9, p. 184, Aug. 2018.

[16] R. L. Hardy, "Multiquadric equations of topography and other irregular surfaces," *Journal of Geophysical Research*, vol. 76, no. 8, pp. 1905-1915, Mar. 1971.

[17] B. R. Franke, "Scattered Data Interpolation: Tests of Some Methods," *Mathematics of Computation*, vol. 48, no. 157, pp. 181-200, Jan. 1982.

[18] F. J. Aguilar, F. Agüera, M. A. Aguilar, F. Carvajal, "Effects of Terrain Morphology, Sampling Density, and Interpolation Methods on Grid DEM Accuracy," *Photogrammetric Engineering and Remote Sensing*, vol. 71, no. 17, pp. 805-816, Jul. 2005.

- [19] S. Chantasiriwan, "Error and variance of solution to the stochastic heat conduction problem by multiquadric collocation method," *International Communications in Heat and Mass Transfer*, vol. 33, no. 3, pp. 342-349, Mar. 2006.
- [20] J. Sun, K. Luo, H. L. Yi, H. P. Tan, "Local multiquadric RBF meshless scheme for radiative heat transfer in strongly inhomogeneous media," *Journal of Quantitative Spectroscopy and Radiative Transfer*, vol. 164, pp. 54-68, Oct. 2015.
- [21] Z. C. Zheng, W. Li, "Numerical stabilities and boundary conditions in time-domain Eulerian simulations of acoustic wave propagations with and without background flow," *Applied Mathematics and Computation*, vol. 202, no. 1, pp. 146-161, 2008.
- [22] A. Y. Dong, S. H. Lo, Y. K. Cheung, "Numerical solution for elastic inclusion problems by domain integral equation with integration by means of radial basis functions," *Engineering Analysis with Boundary Elements*, vol. 28, no. 6, pp. 623-632, Jun. 2004.
- [23] A. Golbabai, E. Mohebianfar, "A new method for evaluating options based on multiquadric RBF-FD method," *Applied Mathematics and Computation*, vol. 308, pp. 130-141, Sep. 2017.
- [24] F. Soleymani, U. Z. Malik, "A multiquadric RBF-FD scheme for simulating the financial HHW equation utilizing exponential integrator," *Calcolo*, vol. 55, p. 51, Nov. 2018.
- [25] J. MacQueen, "Some Methods for Classification and Analysis of MultiVariate Observations," *Proceedings of the fifth Berkeley symposium on mathematical statistics and probability*, Berkeley, 1967, pp. 281-297.
- [26] J. J. Tang, S. Zhang, X. Q. Chen, F. Liu, Y. J. Zou, "Taxi trips distribution modeling based on Entropy-Maximizing theory: A case study in Harbin city-China," *Physica A*, vol. 493, pp. 430-443, Mar. 2017.
- [27] X. B. Wu, N. Chi, "The phase estimation of geometric shaping 8-QAM modulations based on K-means clustering in underwater visible light communication," *Optics Communications*, vol. 444, pp. 147-153, Aug. 2019.
- [28] Y. X. Du, B. Sun, R. Q. Lu, C. L. Zhang, H. Wu H, "A method for detecting high-frequency oscillations using semi-supervised k-means and mean shift clustering," *Neurocomputing*, vol. 350, pp. 102-107, Jul. 2019.
- [29] [29] Zhu Q, Pei J, Liu XB, Zhou ZP. Analyzing commercial aircraft fuel consumption during descent: A case study using an improved K-means clustering algorithm. *J Clean Prod*. 2019;223: 869-882.
- [30] W. Kuśmirek, A. Szmurlo, M. Wiewiórka, R. Nowak, T. Gambin, "Comparison of kNN and k-means optimization methods of reference set selection for improved CNV callers performance," *BMC Bioinformatics*, vol. 20, p. 266, May 2019.
- [31] R. K. Esfahani, F. Shahbazi, M. Akbarzadeh, "Three phase classification of an uninterrupted traffic flow: a k-means clustering study," *Transportmetrica B*, vol. 7, no. 1, pp. 546-558, Mar. 2019.
- [32] A. D. Dubey, "K-Means based radial basis function neural networks for rainfall prediction," *International Conference on Trends in Automation, Communications and Computing Technology, IEEE, Bangalore*, 2015, p. 16091616.
- [33] X. P. Yang, Y. Q. Li, Y. Z. Sun, T. Long, T. K. Sarkar, "Fast and robust RBF neural network based on global K-means clustering with adaptive selection radius for sound source angle estimation," *IEEE Transactions on Antennas and Propagation*, vol. 66, no. 6, pp. 3097-3107, Jun. 2018.
- [34] E. K. Smith, S. Weintraub, "The constants in the equation for atmospheric refractive index at radio frequencies," *Proceedings of the IRE*, vol. 41, no. 8, pp. 1035-1037, Aug. 1953.

Tao Ma was born in Nanyang, Henan Province, China. He received the master's degree in electronic and information engineering from microelectronics and solid-state electronics from South China Normal University, Guangzhou, China, in 2005, and received the PhD degree in optical engineering from Beijing University of Posts and Telecommunications, Beijing, China, in 2017. His current research interests include electromagnetic metamaterial, micro-nano ring resonance, optoelectronic device and optical sensing.

Heng Liu was born in Xinxiang, Henan Province, China. She received the bachelor's degree in information and computing science from Henan Normal University, Xinxiang, China, in 2001. Shanghai, China, and received the master's degree in computer software and theory from Shanghai Maritime University, Shanghai, China, in 2006. Her current research interests include pattern recognition, image retrieval and computer aided modeling.

Yu Zhang was born in Qinyang, Henan Province, China. He received the bachelor's degree in electromagnetic field and microwave technology from Xidian University, Xi'an, China, in 1986. He is a senior member of China electronics association. From 1986 to 2005, he was a senior engineer in China institute of radio communication, Xinxiang, China. From 2000 to the present, he was a professor in Henan Normal University, Xinxiang, China. He has authored or co-authored over 40 papers and undertook the completion of the national 863 projects and Military projects. His current research interests include radar technology, atmospheric refractivity error correction, electromagnetic wave detection and propagation and radio frequency identification technology.